Non-interferometric and non-iterative complex wave-field reconstruction based on Kramers-Kronig relations

Shen, Cheng, Zhou, Haowen, Yang, Changhuei

Cheng Shen, Haowen Zhou, Changhuei Yang, "Non-interferometric and non-iterative complex wave-field reconstruction based on Kramers-Kronig relations," Proc. SPIE 11970, Quantitative Phase Imaging VIII, 1197002 (2 March 2022); doi: 10.1117/12.2608280

SPIE.

Event: SPIE BiOS, 2022, San Francisco, California, United States

Non-interferometric and non-iterative complex wave-field reconstruction based on Kramers-Kronig relations

Cheng Shen*[a], Haowen Zhou[a], Changheui Yang[a]
[a]Department of Electrical Engineering, California Institute of Technology, Pasadena, CA USA 91125

ABSTRACT

We reported a novel non-interferometric and non-iterative computational imaging method, synthetic aperture imaging based on Kramers-Kronig relations (KKSAI), to reconstruct complex wave-field. By collecting images through a modified microscope system with pupil modulation capability, we show that the phase and amplitude profile of the sample at pupil limited resolution can be extracted from as few as two intensity images by exploiting Kramers-Kronig relations. KKSAI reconstruction is non-iterative, free of parameter tuning and applicable to a wider range of samples. Simulation and experiment results have proved that it has much lower computational burden and achieves the best reconstruction quality when compared with two existing phase imaging methods.

Keywords: Coherent imaging, phase retrieval, Kramers-Kronig relations

1. INTRODUCTION

Coherent imaging techniques are playing a growingly essential role in varieties of fields including cellular biophysics [1], digital pathology [2], and X-ray crystallography [3] to name a few. They aim to obtain the complex wave-field and its difficulty lies in the quantitative phase measurement since the frequency of working wavelength usually massively exceeds the maximum response speed of even state-of-the-art detectors. Nevertheless, the intensity measurement is easy. Thus, much effort from optical imaging community has been put into inferring phase information from purely intensity measurements over the past decades. The existing quantitative phase measurement methods can be generally categorized as two groups, interferometric and non-interferometric ones. The former includes digital holography [4], phase shifting interferometry [5], and optical coherence tomography [6]. Iterative phase (diversity) retrieval [7–10], (Fourier) ptychography [11–15], transport of intensity equation [16, 17], and quantitative differential phase contrast [18–20] belong to the latter. Non-interferometric methods are inherently attractive, as they are generally simpler to implement and more robust to use. However, they either rely on some assumption on objects of interest and further approximation or suffer from the heavy data volume and convergence-unguaranteed non-convex optimization. In this manuscript, we reported an innovative non-interferometric and non-iterative coherent imaging modality named as synthetic aperture imaging based on Kramers-Kronig relations (KKSAI), which requires as few as two measurements. We compared it with two existing methods, pupil modulation Fourier ptychographic microscopy (PM-FPM) [13] and pupil modulation quantitative differential phase contrast (PM-DPC) microscopy [20], and proved that our proposed method can achieve better complex wave-field reconstruction with the same measurements.

2. METHODS

2.1 Experimental setup

Figure 1(a) illustrates the schematic of our KKSAI imaging system. It is adapted from a conventional wide-field microscope by relaying the back focal plane of objective (10X Mitutoyo Plan Apo infinity corrected objective, 0.28 NA) onto a reflective spatial light modulator (Holoeye LC-R 1080) to achieve amplitude pupil modulation. Also, a pair of linear polarizers (P1 and P2) are needed to maximize the modulation contrast with their polarization directions orthogonal to each other. The pixel size of the camera (Allied Vision Prosilica GX 6600) is 5.5 μm. The illumination is provided by a laser diode (Thorlabs DJ532-40) with the central wavelength of 532 nm, coupled into a multi-mode fiber (Thorlabs FT200emtcustom, 0.39 NA, Ø200 μm). The fiber is vibrated to wash out the speckle at the camera plane.

*cshen3@caltech.edu

Quantitative Phase Imaging VIII, edited by Yang Liu, Gabriel Popescu, YongKeun Park,
Proc. of SPIE Vol. 11970, 1197002 · © 2022 SPIE · 1605-7422 · doi: 10.1117/12.2608280

The system can be simplified as a 4*f* imaging system, as shown in Fig. 1(b). We denote the coordinates on the pupil plane and the camera sensor plane as (*u*, *v*) and (*x*, *y*) respectively. According to the property of Fourier transform, the coordinates on the sample plane should be (-*x*, -*y*). If the complex-valued sample *s*(-*x*, -*y*) in Fig. 1(c) is placed, its detectable spectrum by this system at the pupil-limited resolution is

$$S(u,v) = F\{s\}(u,v) \cdot C(u,v), \tag{1}$$

where $F\{\cdot\}$ is the Fourier transform (FT) operator and $C(u,v)$ is the coherent transfer function (CTF) of imaging system as indicated by the red circle in Fig. 1(d). Its radius is determined by the objective numerical aperture (NA). Our overarching objective is to recover $S(u,v)$.

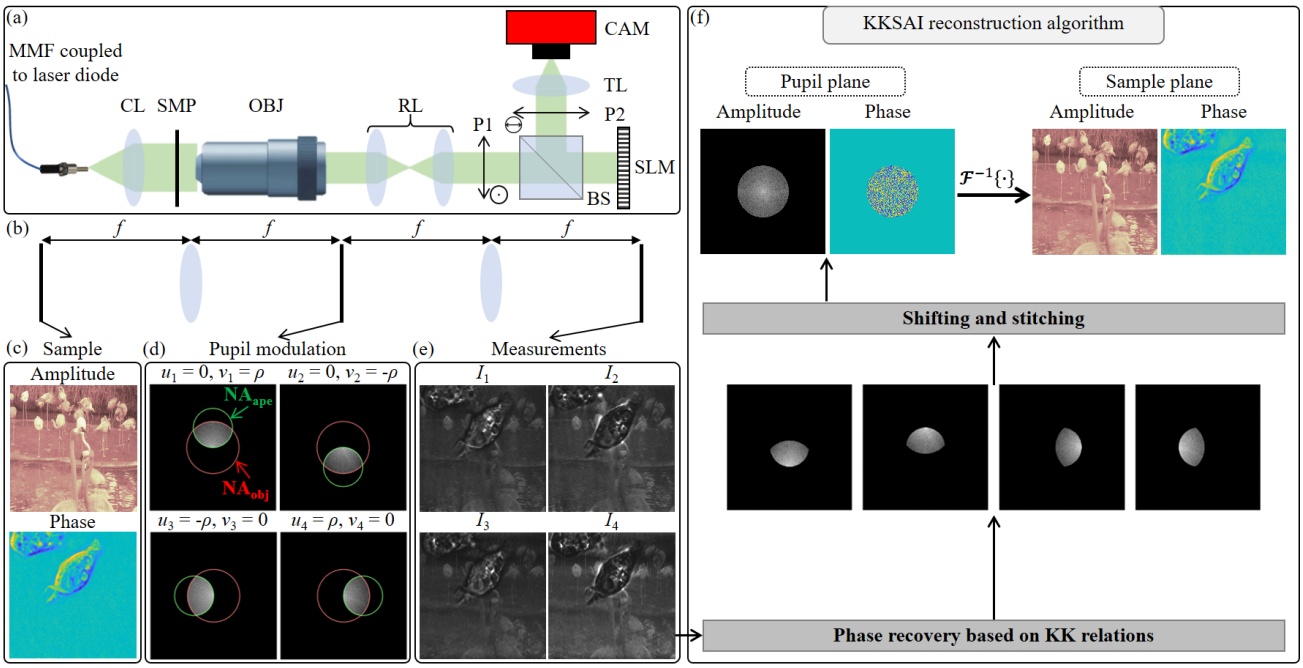

Figure 1. KKSAI principle. (a) Experimental setup schematic. (b) Simplified 4*f* system corresponding to (a). (c) Simulated complex-valued sample. (d) Amplitude pupil modulation indicated by the green circle, whose center is (u_i, v_i). (e) Measured intensity images corresponding to (d). (f) KKSAI reconstruction algorithm flowchart. It finally recovers the pupil-limited sample spectrum. MMF, multi-mode fiber; CL, collimating lens; SMP, sample; OBJ, objective; RL, relay lens; P, polarizer; BS, beam splitter; SLM, spatial light modulator; TL, tube lens; CAM, camera.

2.2 Data acquisition

During measurement, a binary circular aperture $D(u,v)$ is scanned at the pupil plane and its edge strictly crosses the pupil center, indicated by green circles in Fig. 1(d). We use four scanning steps to fully cover $S(u,v)$ and its offset distance from the pupil center is ρ. At each step, the scanning aperture can be denoted as $D(u-u_i, v-v_i), i = 1,2,3,4$, and its cropped sub-region from sample spectrum is

$$S_i(u,v) = S(u,v) \cdot D(u-u_i, v-v_i). \tag{2}$$

Its corresponding intensity measurement will be

$$I_i(x,y) = \left| F^{-1}\{S_i(u,v)\} \right|^2. \tag{3}$$

2.3 Reconstruction algorithm

The main goal of the KKSAI reconstruction algorithm is to recover the complex-valued $S_i(u,v)$ from $I_i(x,y)$. One key observation is that the Fourier spectrum of $I_i(x,y)$ is comparable to the one of off-axis hologram, which is due to superposition of the unscattered planar wave and the scattered field from sample.

$$I_i(x,y) = \left|F^{-1}\left\{S_i(u,v)\right\}\right|^2 = \left|F^{-1}\left\{S_i'(u,v) + \delta(u,v)\right\}\right|^2 = \left|s_i'(x,y) + e^{-j(0\cdot x + 0\cdot y)}\right|^2, \tag{4}$$

where $s_i'(x,y)$ is the scattered field exiting from the sample plane and $e^{-j(0*x+0*y)}$ represents the ballistic light going through the sample. Thus, we can adapt a new finding reported for off-axis holography [21] to perform phase recovery. It is based on Kramers-Kronig (KK) relations.

Taking $I_1(x,y)$ as the example, we first generate the hypothetical reference plane wave, which is determined by the offset of $S_1(u,v)$ and in turn by the scanning aperture position (u_1,v_1). For $I_1(x,y)$, it is expressed as

$$r_1(x,y) = F^{-1}\left\{\delta(u+u_1, v+v_1)\right\} = e^{-j(u_1\cdot x + v_1\cdot y)}. \tag{5}$$

Next, a Hilbert kernel is specified as

$$H_1(u,v) = -j\cdot sgn(v_1)\cdot sgn(v), \tag{6}$$

where $sgn(v)$ is the sign function. And an intermediate variable is defined as

$$X = \ln\left(\frac{F^{-1}\left\{S_1(u+u_1, v+v_1)\right\}}{r_1(x,y)}\right). \tag{7}$$

Then,

$$\mathrm{Re}\{X\} = \frac{1}{2}\ln\left(\frac{I_1(x,y)}{\left|r_1(x,y)\right|^2}\right), \tag{8}$$

$$\mathrm{Im}\{X\} = F^{-1}\left\{F\left\{\mathrm{Re}\{X\}\right\}\cdot H_1(u,v)\right\}, \tag{9}$$

where $\mathrm{Re}\{\cdot\}$ and $\mathrm{Im}\{\cdot\}$ are the operator to take real part and imaginary part from a complex value respectively. Thus,

$$S_1(u+u_1, v+v_1) = F\left\{e^{\mathrm{Re}\{X\}+j\cdot\mathrm{Im}\{X\}}\cdot r_1(x,y)\right\}. \tag{10}$$

After obtaining the shifted version of four sub-regions, we can move them back to the correct position and get

$$S_i(u,v), i = 1,2,3,4. \tag{11}$$

Eventually,

$$S(u,v) = \frac{\sum_{i=1}^{4} S_i(u,v)}{\varepsilon + \sum_{i=1}^{4} D(u-u_i, v-v_i)}, \tag{12}$$

where $\varepsilon = 10^{-5}$ is a small constant for numerical stability in the zero-valued region. As seen in Fig. 1(f), the reconstruction results of KKSAI are in good agreement with the original sample function. The validity of this KK-relations-based process has been demonstrated in the original paper [21] for off-axis holography. It leverages the analyticity of band-limited signals. Its extendibility to KKSAI has then been proved in [22].

2.4 Scanning scheme

Figure 2(b1) shows the scanning scheme discussed above. It is designed to cover the entire pupil but with some overlap. It is not the most efficient since redundancy is not necessary for KKSAI. In principle, as long as the scanning of any convex aperture covers the whole pupil and its edge crosses the origin, the scanning scheme should work for KKSAI [22]. We can choose a rectangular aperture with 2 non-overlapping measurements shown in Fig. 2(c1). The two scans have aperture edge exactly cross the pupil origin.

3. RESULTS AND DISCUSSION

3.1 Simulation

We first conducted simulations to compare the complex wave-field reconstruction performance of our proposed method with two existing imaging modalities, PM-DPC [20] and PM-FPM [13]. For fairness, all the three methods in the following discussions utilize the same dataset.

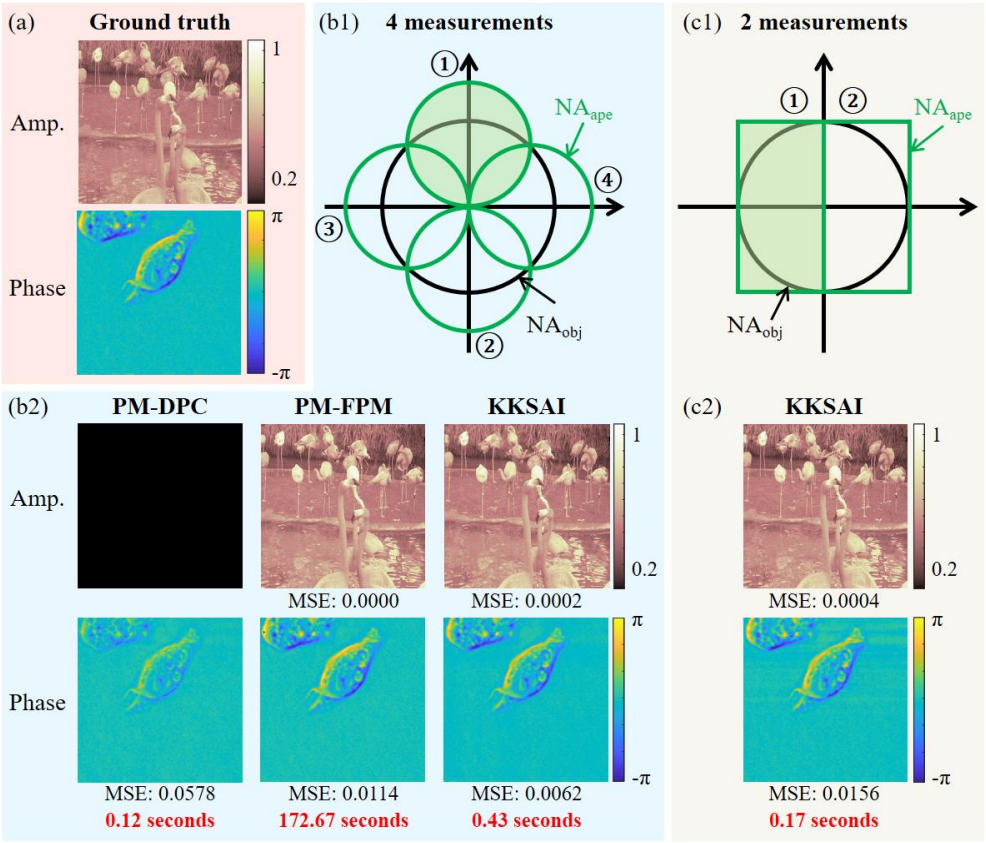

Figure 2. Simulation results. (a) Amplitude (Amp.) and phase distribution of simulated complex-valued sample; Complex wave-field reconstruction (b2) of two existing methods, PM-DPC and PM-FPM, as well as the proposed KKSAI from four intensity measurements by the scanning scheme (b1); Complex wave-field reconstruction (c2) of KKSAI from only two measurements by the scanning scheme (c1). Both (b1) and (c1) cover the entire pupil with green shade indicating the passing band on pupil plane during scanning, where ⓘ is used to label the measurement sequence. Under each reconstruction is the MSE metric between it and ground truth.

We simulated a complex-valued sample. Its amplitude and phase are displayed in Fig. 2(a). Under the scanning scheme in Fig. 2(b1), PM-DPC fails badly as it is incapable of recovering amplitude. Moreover, the large sample phase variations violate the weak sample assumption required for PM-DPC reconstruction. Not surprisingly, it provides a poor phase rendering in this case. PM-FPM and KKSAI obtained phase and amplitude reconstruction of similar quality. However, PM-FPM requires good initialization and careful parameter tuning to arrive at the correct result. Furthermore, it takes around 400 times longer to converge to the current result when compared to KKSAI. When it comes to the

scanning scheme in Fig. 2(c1), KKSAI still obtains satisfactory reconstruction. To quantitatively compare them, the mean square error (MSE) between each reconstruction and the ground truth is calculated and labelled under each image.

3.2 Experiment

Next, we conducted the imaging experiments using a papillary thyroid carcinoma Pap smear slide with papanicolaou stain. It is a complex-valued sample. Figure 3(a) displays two raw images from two different scanning schemes for the region of interest (ROI). Due to the pupil amplitude modulation, the shade effect can be seen in the measurements and it is clear that their spectrum contains two cross-interference terms similar to those of an off-axis hologram.

To obtain the ground truth for this complex-valued sample, we performed a separate PM-FPM experiment where 47 pupil modulation images with an overlapping rate of about 85% in Fourier domain were acquired. Its high-resolution reconstruction shown in Fig. 3(b) is taken as the ground truth to evaluate the performance of three methods. As we can see in Fig. 3(c), PM-DPC cannot recover amplitude and PM-FPM reconstructions based on four measurements are of poor quality. Comparing to the noise-free simulation case, the FPM algorithm suffers from the low overlapping rate in Fourier domain and in turn insufficient redundancy to be robust to the noise in the real experiments. With naked eyes' evaluation, both amplitude and phase recovery of KKSAI are the closest to ground truth. Even when only two measurements are used, the reconstruction quality of KKSAI is still comparable to the one from four measurements. Quantitatively, we calculated the feature similarity (FSIM) index [23] between reconstruction and ground truth and reported them under each image. The quantitative results are in accordance with our observation.

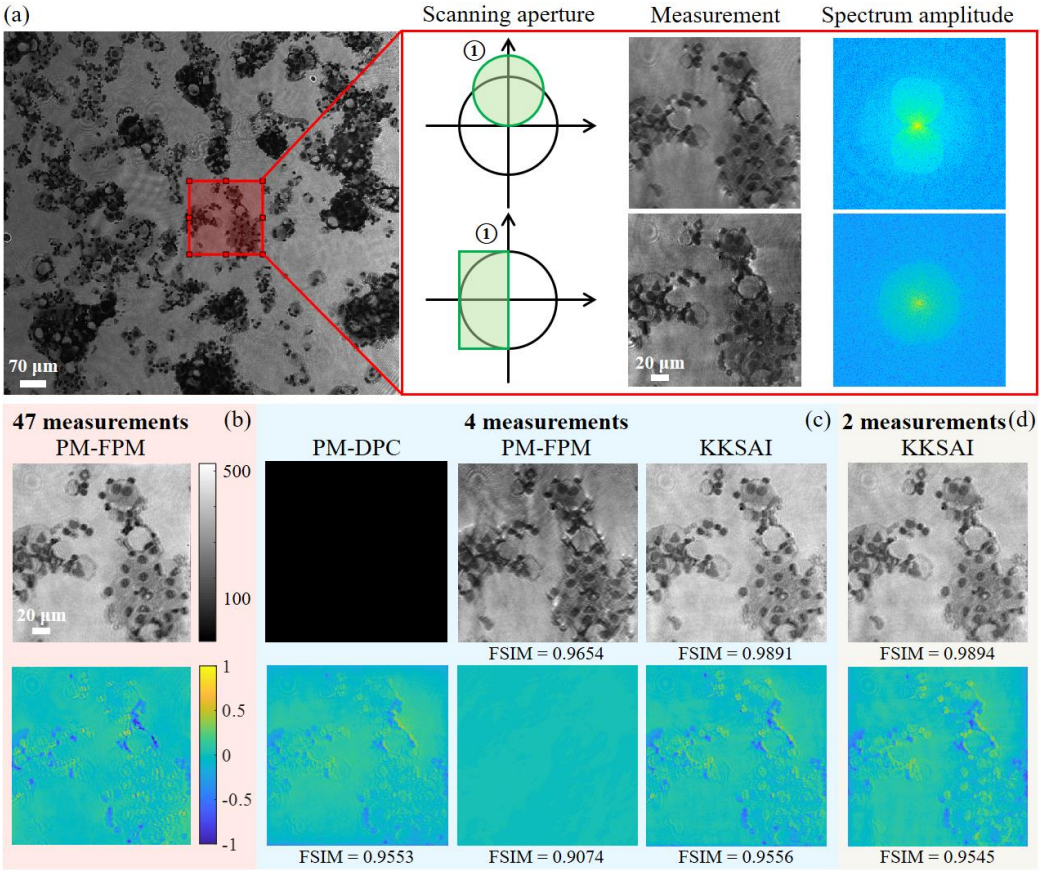

Figure 3. Experiment results. (a) Display of the ROI patch in a Pap smear slide and one of the measurements under two scanning schemes as well as their Fourier amplitude spectrum. (b) Complex wave-field reconstruction by PM-FPM from 47 measurements, which will be used as ground truth for evaluation (Top: amplitude; Bottom: phase). (c) Complex wave-field reconstruction by PM-DPC, PM-FPM and KKSAI from 4 measurements by the scanning scheme Fig. 2(b1). (d) Complex wave-field reconstruction by KKSAI from 2 measurements by the scanning scheme Fig. 2(c1). Under each reconstruction is the FSIM metric between it and ground truth.

3.3 Noise robustness test

During experiment, the noise robustness of our proposed KKSAI was also tested in comparison with the other two existing methods. A simple way to vary the noise level in measurements is to adjust the exposure time of camera. As the exposure time is shortened, the shot noise will increase. The results are summarized in Fig. 4(a). It shows that as the noise level increases, both amplitude and phase recovery of all the three methods becomes worse. However, KKSAI maintains the best all the way. Figure 4(b) displays the case when the exposure time is $5\times10^5\,\mu s$. Clearly, it confirms that KKSAI is most robust to experimental noise. Besides, it needs to be pointed out that when the exposure time reaches to $1\times10^6\,\mu s$, all the reconstructions become slightly worse than the one under $5\times10^5\,\mu s$ because of the overexposure.

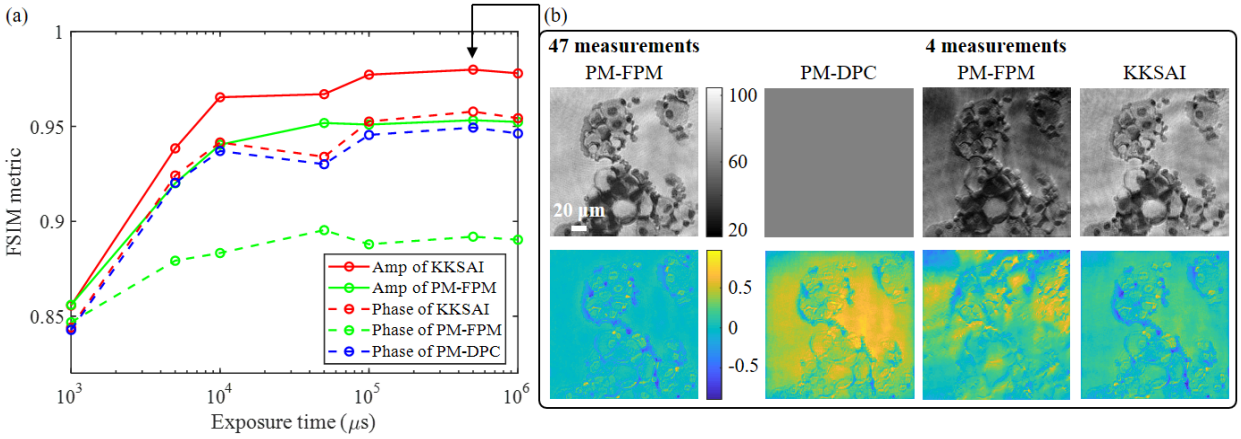

Figure 4. Noise robustness test of different methods. (a) As exposure time decreases, the noise level in measurements is increasing. Complex wave-field reconstruction of all three methods becomes worse. However, KKSAI maintains the best in both amplitude and phase recovery. (b) Demonstration when exposure time is $5\times10^5\,\mu s$.

4. CONCLUSION

In this manuscript, a new complex wave-field imaging method, KKSAI, is reported. Its experimental setup, data acquisition and reconstruction algorithm are described in detail. A recent advance for off-axis holography based on KK relations [21] is adapted here to recover phase from intensity images in a non-interferometric way by leveraging the analyticity of band-limited signals under pupil modulation. As a computational imaging modality, KKSAI co-designs the sensing part and the reconstruction algorithm. From the perspective of sensing, it requires much fewer measurements than PM-FPM. From the perspective of reconstruction, it is iteration-free and does not require any sample priors, and is thus more generally usable than PM-DPC. Our simulation and experiment results demonstrate that KKSAI has clear advantages over the other two methods. We hope KKSAI can find more application in the coherent imaging field.

5. ACKNOWLEDGEMENTS

Authors thank Ruizhi Cao for helpful discussions on this work. This project is supported by Rosen Center Pilot Grant Award 9900050.

REFERENCES

[1] Y. Park, M. Diez-Silva, G. Popescu, G. Lykotrafitis, W. Choi, M. S. Feld, and S. Suresh, “Refractive index maps and membrane dynamics of human red blood cells parasitized by plasmodium falciparum,” Proc. Natl. Acad. Sci. 105(37), 13730-13735 (2008).

[2] A. Greenbaum, Y. Zhang, A. Feizi, P.-L. Chung, W. Luo, S. R. Kandukuri, and A. Ozcan, “Wide-field computational imaging of pathology slides using lens-free on-chip microscopy,” Sci. Translational Medicine 6(267), 267ra175-267ra175 (2014).

[3] J. Miao, D. Sayre, and H. Chapman, "Phase retrieval from the magnitude of the Fourier transforms of nonperiodic objects," JOSA A 15(6), 1662-1669 (1998).
[4] G. Popescu, T. Ikeda, R. R. Dasari, and M. S. Feld, "Diffraction phase microscopy for quantifying cell structure and dynamics," Opt. Letters 31(6), 775-777 (2006).
[5] N. T. Shaked, Y. Zhu, M. T. Rinehart, and A. Wax, "Two-step-only phase-shifting interferometry with optimized detector bandwidth for microscopy of live cells," Opt. Express 17(18), 15585-15591 (2009).
[6] Z. Yaqoob, W. Choi, S. Oh, N. Lue, Y. Park, C. Fang-Yen, R. R. Dasari, K. Badizadegan, and M. S. Feld, "Improved phase sensitivity in spectral domain phase microscopy using line-field illumination and self phase-referencing," Opt. Express 17(13), 10681-10687 (2009).
[7] R. W. Gerchberg, "A practical algorithm for the determination of phase from image and diffraction plane pictures," Optik 35, 237-246 (1972).
[8] J. R. Fienup, "Phase retrieval algorithms: a comparison," Appl. Optics 21(15), 2758-2769 (1982).
[9] C. Shen, X. Bao, J. Tan, S. Liu, and Z. Liu, "Two noise-robust axial scanning multi-image phase retrieval algorithms based on pauta criterion and smoothness constraint," Opt. Express 25(14), 16235-16249 (2017).
[10] C. Guo, C. Shen, J. Tan, X. Bao, S. Liu, and Z. Liu, "A robust multi-image phase retrieval," Optics and Lasers in Engineering 101, 16-22 (2018).
[11] J. M. Rodenburg and H. M. Faulkner, "A phase retrieval algorithm for shifting illumination," Appl. Physics Letters 85(20), 4795-4797 (2004).
[12] G. Zheng, R. Horstmeyer, and C. Yang, "Wide-field, high-resolution Fourier ptychographic microscopy," Nat. Photonics 7(9), 739-745 (2013).
[13] X. Ou, J. Chung, R. Horstmeyer, and C. Yang, "Aperture scanning Fourier ptychographic microscopy," Biomed. Optics Express 7(8), 3140-3150 (2016).
[14] C. Shen, A. C. S. Chan, J. Chung, D. E. Williams, A. Hajimiri, and C. Yang, "Computational aberration correction of VIS-NIR multispectral imaging microscopy based on Fourier ptychography," Optics Express 27(18), 24923-24937 (2019).
[15] G. Zheng, C. Shen, S. Jiang, P. Song, and C. Yang, "Concept, implementations and applications of Fourier ptychography," Nat. Reviews Physics 3(3), 207-223 (2021).
[16] L. Waller, L. Tian, and G. Barbastathis, "Transport of intensity phase amplitude imaging with higher order intensity derivatives," Opt. Express 18(12), 12552-12561 (2010).
[17] C. Zuo, Q. Chen, Y. Yu, and A. Asundi, "Transport-of-intensity phase imaging using savitzky-golay differentiation filter-theory and applications," Opt. Express 21(5), 5346-5362 (2013).
[18] S. B. Mehta and C. J. Sheppard, "Quantitative phase-gradient imaging at high resolution with asymmetric illumination-based differential phase contrast," Opt. Letters 34(13), 1924-1926 (2009).
[19] L. Tian and L. Waller, "Quantitative differential phase contrast imaging in an LED array microscope," Opt. Express 23(9), 11394-11403 (2015).
[20] H. Lu, J. Chung, X. Ou, and C. Yang, "Quantitative phase imaging and complex field reconstruction by pupil modulation differential phase contrast," Opt. Express 24(22), 25345-25361 (2016).
[21] Y. Baek, K. Lee, S. Shin, and Y. Park, "Kramers–Kronig holographic imaging for high-space-bandwidth product," Optica 6(1), 45-51 (2019).
[22] C. Shen, M. Liang, A. Pan, and C. Yang, "Non-iterative complex wave-field reconstruction based on Kramers-Kronig relations," Photonics Research 9(6), 1003-1012 (2021).
[23] L. Zhang, L. Zhang, X. Mou, and D. Zhang, "FSIM: A feature similarity index for image quality assessment," IEEE Transactions on Image Process. 20(8), 2378-2386 (2011).